

In situ generated gas bubble-directed self-assembly of multifunctional MgO-based hybrid foams for highly efficient thermal conduction, microwave absorption, and self-cleaning

Feifei You,[†] Xinyu Liu,[†] Meiwan Ying,[†] Yijun Yang,[†] Yutong Ke,[†] Yi Shen,[†] Guoxiu Tong ^{*†} and Wenhua Wu [†]

[†]*College of Chemistry and Material Sciences, Key Laboratory of the Ministry of Education for Advanced Catalysis Materials, Zhejiang Normal University, Jinhua 321004, China.*

* **Corresponding Authors:** E-mail: tonggx@zjnu.cn (G.X. Tong); Tel.: +86-579-82282269; Fax: +86-579-82282269.

Experiment section

Characterization

ZEISS GeminiSEM 300 scanning electron microscope (SEM, 10 kV) and a Horiba EX-250 energy dispersive X-ray spectrometer (EDS) connected with it were applied to analyze the surface morphology, element content and distribution of the MgO/Co/C hybrid foams. A JEM-2100F transmission electron microscope (TEM, 200 kV) was used to further confirm the microstructure of products. A D/MAX-III A X-ray diffractometer (XRD) with X-ray ($\lambda = 0.15418$ nm, came from Cu K α) as the radiation source was employed to record XRD patterns for the phase analysis. The working voltage, working current, and scanning speed were 40.0 kV, 40.0 mA, 4 °/min, respectively. The crystallite sizes and the microstrain level were obtained by analyzing and calculating using jade 6. Fourier transform infrared (FTIR) spectroscopy obtained in the transmission mode within the scanning range from 400 to 4000 cm⁻¹ was used to evaluate the surface functionalities of MgO/Co/C foams, using a Nicolet 8700 Fourier transform infrared spectrometer. The graphitization degree analysis of carbon was executed on a Renishaw RM10000 Raman spectrometer. The oxidation states of surface elements are assessed in the samples using a ESCALAB250 X-ray photoelectron spectroscopy (XPS). To obtain the Brunauer–Emmett–Teller (BET) specific surface area, the N₂ adsorption/desorption isotherm was done on an Autosorb iQ instrument (Quantachrome, Florida, USA), and the sample was outgassed under vacuum at 160 °C

for 8 h.

Contact Angle test and Droplet Rolling Test

To evaluate the hydrophobicity of the MgO/Co/C/silicone films, contact angle test and droplet rolling test were performed. Place the MgO/Co/C/silicone films on the sample table as instructed by the display screen and adjust the “height adjustment knob” and “focal length adjustment knob” to make the films appear clearly in the display. Then, squeeze the needle containing water to make water drop to the surface of the film, and take photos of the hydrophilic angle of water on the surface of the film for recording (40 sheets per second), the instrument type used is SDC-100. For the water drop test, the film is placed on a platform as shown in Fig. S9, and a drop of water is placed on the surface of the film. The plane is tilted by slow lifting, and the inclination Angle of the platform is recorded when the droplet rolls off. Besides, a film was attached to the platform and kept at angle of 6° to carry out the droplet rolling experiment (Movie S1).

Measurement of conductivity, EM parameters, and heat conductance.

The conductivity of the prepared MgO/Co/C foams was evaluated by a four-point probe (RTS-9 model) method. To measure the conductivity, the disc pellets about 7 mm in diameter and 1.0 mm in thickness were formed by pressing the MgO/Co/C foams in a mold.

The as-obtained MgO/Co/C foams were mixed uniformly with molten paraffin in equal amounts (1:1, m/m), and the standard toroidal-shaped specimens were prepared with a mold to determine the EMWAPs. The thickness, outer diameter, and inner diameter of the standardized specimens were ca. 3.5 mm, 7.0 mm, and 3.04 mm, respectively. With the coaxial line method adopted, the permeability ($\mu_r = \mu' - j\mu''$) and permittivity ($\varepsilon_r = \varepsilon' - j\varepsilon''$) were measured using a Keysight N5230A vector network analyzer. Reflection loss (RL) generally representing the EMWAPs are computed by the equation: $RL = 20 \log \left| \frac{\sqrt{\mu_r/\varepsilon_r} \tanh[j(2\pi fd/c)\sqrt{\mu_r\varepsilon_r}] - 1}{\sqrt{\mu_r/\varepsilon_r} \tanh[j(2\pi fd/c)\sqrt{\mu_r\varepsilon_r}] + 1} \right|$, where f , c , and d , correspond to the frequency, light velocity under vacuum, sample thickness, respectively. The attenuation constant (A) and matching constant (Z) are computed based on the formula:

$$A = \frac{\sqrt{2\pi}f}{c} \sqrt{(\mu''\varepsilon'' - \mu'\varepsilon') + \sqrt{(\mu'\varepsilon'' + \mu''\varepsilon')^2 + (\mu''\varepsilon'' - \mu'\varepsilon')^2}} \quad \text{and} \quad Z = \left| \frac{Z_{in}}{Z_0} \right| = \left| \sqrt{\frac{\mu_r}{\varepsilon_r}} \tanh\left(j \frac{2\pi f d}{c} \sqrt{\mu_r \varepsilon_r}\right) \right|, \text{ respectively.}$$

Using a transient plane source (TPS) thermal characterization technique with a Hot Disk Thermal Constant Analyzer TPS 2500 apparatus which meets the ISO Standard 22007e2, the thermal conductivity of the MgO/Co/C foams was analyzed. When performing a measurement, a plane Hot Disk sensor of 5465 is fitted between two pieces of the sample, each one with a plane surface facing the sensor which is used both as a heat source and as a dynamic temperature sensor. By running an electrical current, the temperature of the sensor increases, and the resistance (temperature) increase as a function of time was recorded at the same time to obtain the thermal conductivity. All measurements were carried out at room temperature and the average value of three repeated tests was determined.

Measurement of mechanical properties

The mechanical properties of the MgO/Co/C/silicone films were evaluated by a universal material testing machine (UTM4204, Shenzhen Suns Technology Stock Co., Ltd., Shenzhen, China), with a 10 mm/min compression and tensile rates.

Table S1 The effect of salt type on the morphology of the products

| Salt type | Decomposition temperature (°C) | Morphology | Product type |
|--|--------------------------------|------------|--------------------------|
| Mg(NO ₃) ₂ ·6H ₂ O | 330 | foam | MgO/C |
| Ni(NO ₃) ₂ ·6H ₂ O | 110~310 | foam | Ni/C |
| Mn(NO ₃) ₂ ·4H ₂ O | 160~200 | foam | MnO/C |
| Co(NO ₃) ₂ ·6H ₂ O | 80 | / | Co/C |
| Cu(NO ₃) ₂ ·3H ₂ O | 170 | / | Cu/C |
| Fe(NO ₃) ₃ ·6H ₂ O | 125 | / | FeO/C |
| 90%Mg(NO ₃) ₂ ·6H ₂ O +10% Fe(NO ₃) ₃ ·6H ₂ O | / | foam | MgO/FeO/C |
| 70%Mg(NO ₃) ₂ ·6H ₂ O +30% Ni(NO ₃) ₂ ·6H ₂ O | / | foam | MgO/Ni/C |
| 70%Mg(NO ₃) ₂ ·6H ₂ O +30% Cu(NO ₃) ₂ ·3H ₂ O | / | foam | MgO/Cu/C |
| 70%Mg(NO ₃) ₂ ·6H ₂ O +30% Mn(NO ₃) ₂ ·3H ₂ O | / | foam | MgO/MnO/C |
| 70%Mg(NO ₃) ₂ ·6H ₂ O +7.5%Fe(NO ₃) ₃ ·6H ₂ O +22.5%Ni(NO ₃) ₂ ·6H ₂ O | / | foam | MgO/FeNi ₃ /C |
| 70%Mg(NO ₃) ₂ ·6H ₂ O +15%Fe(NO ₃) ₃ ·6H ₂ O +15%Co(NO ₃) ₂ ·6H ₂ O | / | foam | MgO/FeCo/C |
| 70%Mg(NO ₃) ₂ ·6H ₂ O +15%Co(NO ₃) ₂ ·6H ₂ O +15%Ni(NO ₃) ₂ ·6H ₂ O | / | foam | MgO/CoNi/C |
| MgCl ₂ ·6H ₂ O | 135 | / | / |
| MgCl ₂ ·6H ₂ O +CoCl ₂ ·6H ₂ O | 500~600 | / | / |
| C ₁₀ H ₁₄ NiO ₄ | 220°C | / | / |

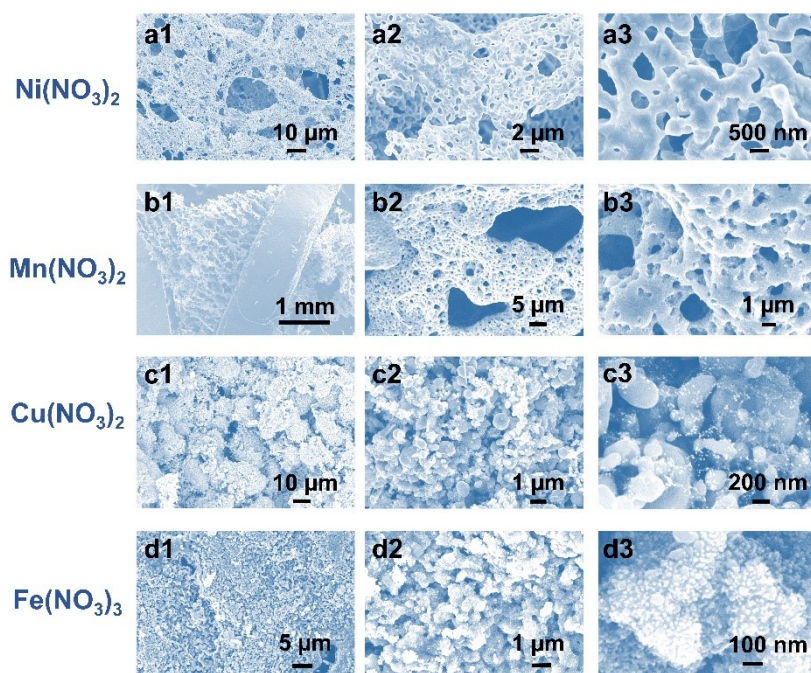


Fig. S1 SEM images of the products using various metal nitrates as raw materials: (a1–a3) $\text{Ni}(\text{NO}_3)_2$, (b1–b3) $\text{Mn}(\text{NO}_3)_2$, (c1–c3) $\text{Cu}(\text{NO}_3)_2$, and (d1–d3) $\text{Fe}(\text{NO}_3)_3$.

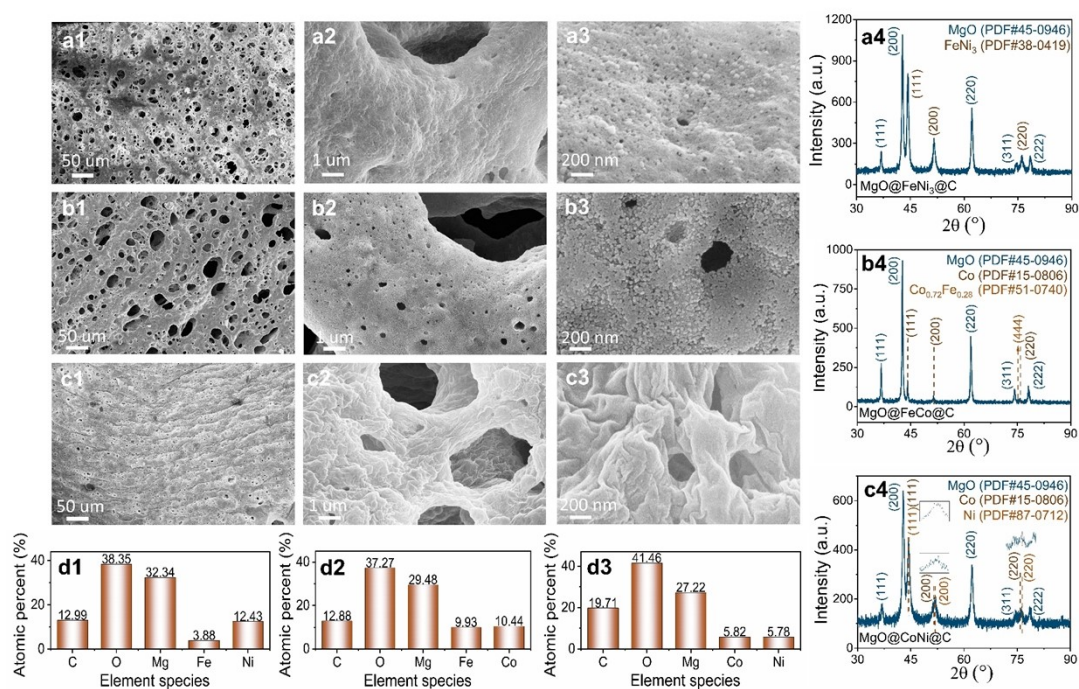


Fig. S2 (a1–a3, b1–b3, and c1–c3) SEM images, (a4–c4) XRD patterns, (d1–d3) element contents of MgO-based foams formed under various nitrates: (a1–a4, d1) $\text{Fe}(\text{NO}_3)_3+\text{Ni}(\text{NO}_3)_2$, (b1–b4, d2) $\text{Fe}(\text{NO}_3)_3+\text{Co}(\text{NO}_3)_2$, and (c1–c4, d3) $\text{Co}(\text{NO}_3)_2+\text{Ni}(\text{NO}_3)_2$.

On the basis of the method mentioned in the article, we changed two kinds of nitrates in the raw material into three kinds of nitrates, one of which is still $\text{Mg}(\text{NO}_3)_2$ ($\varphi = 70$ mol%), and two kinds of $\text{Fe}(\text{NO}_3)_3$, $\text{Co}(\text{NO}_3)_2$ and $\text{Ni}(\text{NO}_3)_2$ were added. Other operations are consistent with the article, and the morphology and composition of the products were analyzed by the results of SEM and XRD, as shown in the above pictures. It can be found from the SEM images (Fig. S2a1–a3, b1–b3, and c1–c3) that all products have a porous foam-like structure and the pore size and surface structure of the foam skeleton varied with the types of nitrates. In the case where $\text{Mg}(\text{NO}_3)_2$ is mixed with $\text{Ni}(\text{NO}_3)_2$ and $\text{Fe}(\text{NO}_3)_3$, the as-obtained foam-like product is a composite of MgO , FeNi_3 , and C (PDF#45-0946 and 38-0419) (Fig. S2a4 and d1). Using the mixtures of $\text{Mg}(\text{NO}_3)_2$, $\text{Co}(\text{NO}_3)_2$ and $\text{Fe}(\text{NO}_3)_3$, the product is $\text{MgO}/\text{CoFe}/\text{C}$ composites (Fig. S2b4 and d2). Moreover, the composites of Mg, Co, Ni and C can be obtained by adding $\text{Mg}(\text{NO}_3)_2$, $\text{Co}(\text{NO}_3)_2$ and $\text{Ni}(\text{NO}_3)_2$ into the reaction system (Fig. S2c4 and d3). In summary, the method has a certain application potential in the preparation of metal alloy doped MgO -based hybrid foams, the formation of metal alloy doped MgO -based hybrid foam may also be affected by factors such as calcination temperature and the proportion of nitrates in the reactants, further exploration is needed.

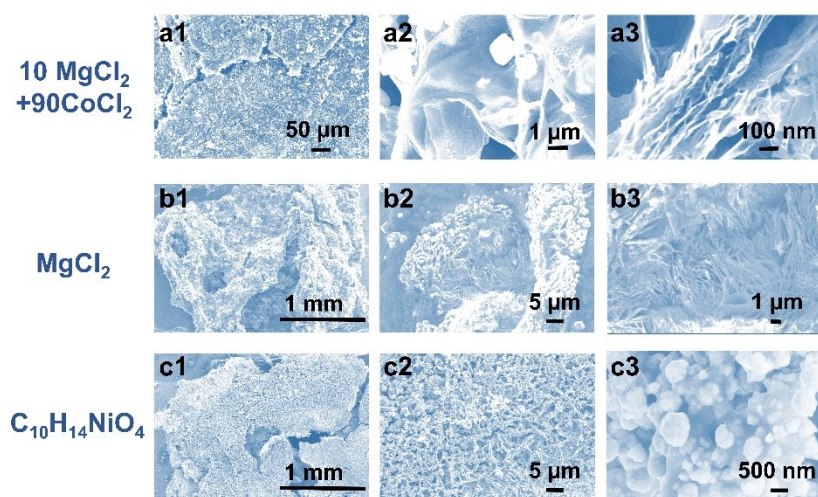


Fig. S3 SEM images of the products using various salts as raw materials.

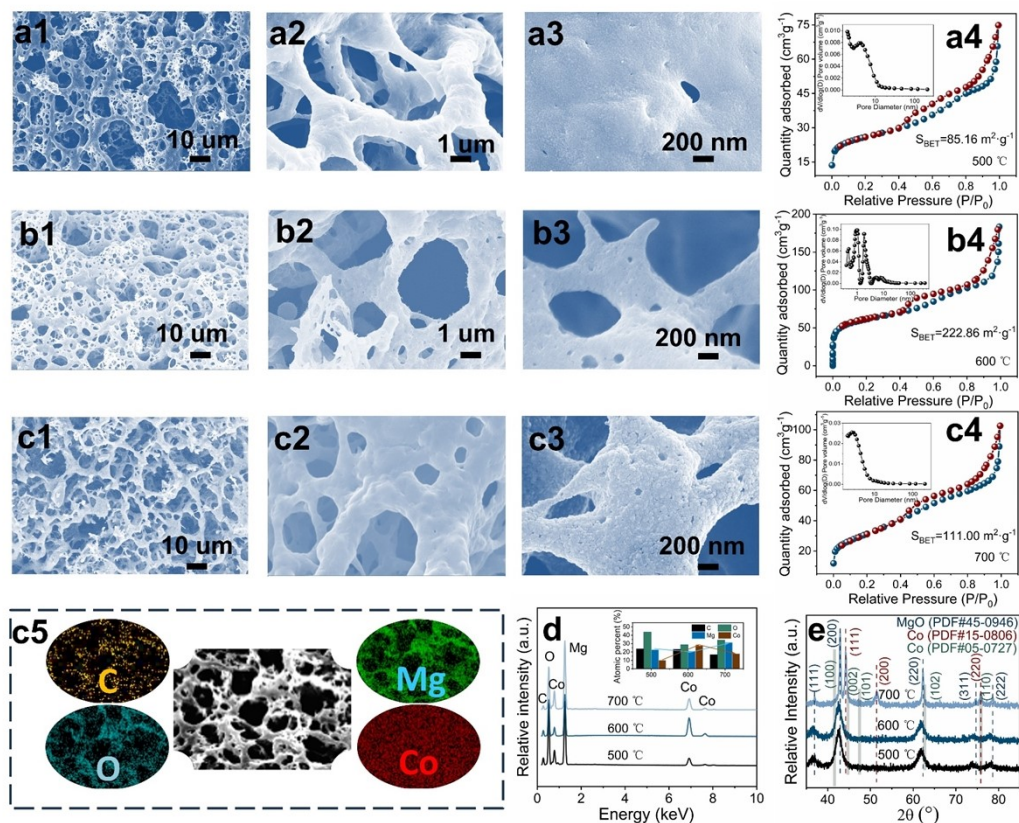


Fig. S4 (a1–a3, b1–b3, c1–c3) SEM images and (a4–c4) N₂ adsorption–desorption isotherms and pore size distribution curves, (c5) element mapping images, and (d) EDX spectra, and (e) XRD patterns of MgO/Co/C foams ($\varphi=30$ mol%) formed under various T_d . (a1–a4) 500°C, (b1–b4) 600°C, and (c1–c5) 700°C.

Seen from Fig. S4a1–a3, b1–b3, c1–c3, the foam-like structure can be kept at $T_d=500^\circ\text{C}\sim 700^\circ\text{C}$. The S_{BET} of MgO/Co/C foams increases from 85.16 cm²/g for 500 °C to 222.86 cm²/g for 600 °C and then decrease to 111.00 cm²/g for 700 °C (Fig. S4a4–c4). Element mapping images and EDX analysis show that the products formed at various T_d consist of Mg, Co, O and C elements (Fig. S4c5 and d). In the XRD patterns (Fig. S4e), all the products contain the same phases (MgO, Co) but various peak intensities. The gradually enhanced peak intensity with T_d means the increased crystallinity and crystallite size. Therefore, controlling T_d can adjust the texture and crystallinity of the foams. A moderate T_d is helpful for the formation of foams with larger S_{BET} .

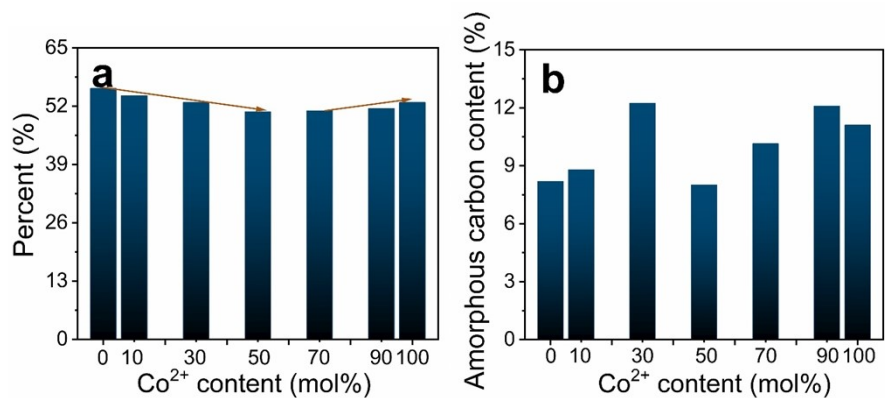


Fig. S5 (a) The proportion of amorphous carbon in the total carbon content calculated from Raman spectra and (b) the content of amorphous carbon in the MgO/Co/C hybrid foams produced under various Co²⁺ contents (φ , mol%) calculated based on Raman and EDX data.

We have calculated the proportion of amorphous carbon in the total carbon content calculated from Raman spectra, as shown in Fig. S5a. Afterward, the content of amorphous carbon phase in MgO/Mg(OH)₂/C and each MgO/Co/C hybrid foam can be calculated based on the results of EDS and Raman, as shown in Fig. S5b.

Table S2 Comprehensive comparison of the *HC* of MgO/Co/C foams with other fillers

| Filler | Matrix | Loading (wt%) | Heat conductivity (W/m·K) | Ref. |
|--|-----------------|---------------|---------------------------|-----------|
| MgO/graphene | epoxy | 31.5 | ~0.51 | 35 |
| MgO | ipp | 30 vol% | ~0.68 | 36 |
| CF-MgO | nylon 6 | 20 | 0.75 | 37 |
| graphite/MgO | PVC | 35 | 0.88 | 38 |
| MgO/BN | epoxy | 45 | 0.92 | 39 |
| MWCNT/MgO | silicone rubber | 30.5 vol% | 1.03 | 40 |
| graphene/Cu-MgO | PCM salt | 50 | 1.34 | 41 |
| MgO | LC epoxy | 33 vol% | 1.41 | 42 |
| g-C ₃ N ₄ @Fe@C hollow micro-polyhedra | silicone | 20 | 1.75 | 11 |
| BN/MgO | fluorosilicone | 60 vol% | 1.82 | 43 |
| AH-MgO | epoxy | 20 | 1.88 | 44 |
| TiO ₂ /Fe/C nanocomposites | silicone | 45 | 2.19 | 7 |
| Ti ₃ C ₂ T _x microflakes | silicone | 50 | 2.75 | 9 |
| γ-Al ₂ O ₃ @Ni@C | silicone | 30 | 2.84 | 5 |
| MgO | EMC | 56 vol% | 3.00 | 45 |
| Al ₂ O ₃ /MgO/GNPs | PC-ABS | 70 | 3.11 | 46 |
| Fe-doped CeO ₂ /Ce(OH) ₃ | silicone | 45 | 3.44 | 2 |
| MgO/EG | MP-LA | 100 | 4.57 | 47 |
| MgO-CoO solid solution | / | 100 | ~2.66 | 48 |
| Mg ₁₀₀ Co ₀ -600°C | silicone | 20 | 2.85 | This work |
| | silicone | 30 | 3.19 | |
| | silicone | 40 | 3.25 | |
| | silicone | 50 | 3.87 | |
| Mg ₉₀ Co ₁₀ -600°C | silicone | 50 | 3.99 | |
| Mg ₇₀ Co ₃₀ -600°C | silicone | 50 | 4.10 | |
| Mg ₅₀ Co ₅₀ -600°C | silicone | 50 | 4.27 | |
| Mg ₃₀ Co ₇₀ -600°C | silicone | 20 | 3.40 | |
| | silicone | 30 | 3.48 | |
| | silicone | 40 | 3.58 | |
| | silicone | 50 | 4.09 | |
| Mg ₁₀ Co ₉₀ -600°C | silicone | 50 | 4.05 | |
| Mg ₀ Co ₁₀₀ -600°C | silicone | 50 | 3.06 | |

Table S3 A EMWAP comparison of MgO/Co/C composites with other absorbers

| Specimens | Filling mass fraction (wt%) | RL _{min} (dB) | f (GHz) (optimal R_L) | d (mm) | EAB (GHz) (RL ≤ -10 dB) | ABW/ d (GHz/m) | Ref. |
|---|-----------------------------|------------------------|----------------------------|----------|------------------------------|------------------|-----------|
| MgO/BaFe ₁₂ O ₁₉ | 70 | -41.0 | 4.27 | 6.0 | ~ 3.0 | 0.50 | 49 |
| LiCo _{0.94} Mg _{0.06} O ₂ /MgO | 40 | ~-10.8 | ~ 8.9 | 2.0 | ~1.1 | 0.55 | 18 |
| MgFe ₂ O ₄ /MgO/C/MoS ₂ | 40 | -56.9 | 9.5 | 2.7 | 3.9 | 1.44 | 50 |
| 10% Ni-doped CeOHCO ₃ | 50 | -35.84 | 13.68 | 2.3 | 4.4 | 1.91 | 31 |
| MgO/carbon | 30 | ~-15.0 | ~12.9 | 2.0 | ~ 4.6 | 2.30 | 51 |
| TiO ₂ /C (MIL-125) | 60 | -47.6 | 16.82 | 1.5 | 3.6 | 2.40 | 52 |
| graphene/chiral PPy/Al ₂ O ₃ | 55 | -60.63 | 15.44 | 2.0 | 5.4 | 2.70 | 10 |
| Fe ₃ O ₄ /C | 60 | -55.43 | 13.76 | 1.7 | ~4.7 | 2.76 | 53 |
| FeSiAl/MgO | 80 | -21.55 | 12.84 | 1.5 | 5.25 | 3.50 | 54 |
| CuFe ₂ O ₄ /MgO | 50 | -25.4 | 8.4 | 2.0 | 8.0 | 4.00 | 21 |
| Fe/MgO | 96 | -65.6 | 12.0 | 2.5 | 14.1 | 5.64 | 55 |
| Co _{0.99} Cu _{0.01} | 30 | -37.94 | 15.87 | 1.3 | 9.68 | 7.45 | 14 |
| C/Co | 25 | -42.36 | 16.4 | 1.9 | 9.84 | 5.18 | 30 |
| Co/C/Fe/C | 40 | -41.97 | 15.2 | 1.55 | 5.28 | 3.41 | 15 |
| Co/CMF foam | 30 | -33.2 | ~14.1 | 2 | 4.8 | 2.40 | 56 |
| TiN/Co@CNFs | 100 | -93 | / | 0.18 | 8.2-12.4 GHz | / | 57 |
| Co/C@MoS ₂ | 30 | -52.76 (2.5mm) | 8.88 | 1.5 | 3.84 | 2.56 | 58 |
| Co/C | 40 | -42 | 7.54 | 3 | ~11.3 | 3.77 | 59 |
| Ni/Co@C | 40 | -66.3 (2.0mm) | 16.4 | 2.3 | 6.02 | 2.62 | 60 |
| Co/C | 50 | -56.3 (2.29mm) | 12.1 | 2 | ~5.8 | 2.9 | 61 |
| CeO ₂ /Co/C | 50 | -20.12 | 14.56 | 1.53 | 4.16 | 2.72 | 62 |
| Co@C/CG | 30 | -45.02 | 14.88 | 1.5 | 4.02 | 2.68 | 63 |
| Mg ₁₀₀ Co ₀ -600°C | 50 | -55.58 (2.5mm) | 15.68 | 2.6 | 4.8 | 1.85 | This work |
| Mg ₉₀ Co ₁₀ -600°C | 50 | -40.00 | 11.2 | 3.0 | 9.2 | 3.07 | |
| Mg ₇₀ Co ₃₀ -600°C | 50 | -32.17 (2.0mm) | 15.52 | 2.2 | 5.6 | 2.55 | |
| Mg ₅₀ Co ₅₀ -600°C | 50 | -53.67 (3.8mm) | 9.6 | 3.1 | 9.76 | 3.15 | |
| Mg ₃₀ Co ₇₀ -600°C | 50 | -41.60 | 11.76 | 2.4 | 11.92 | 4.97 | |
| Mg ₁₀ Co ₉₀ -600°C | 50 | -59.42 | 6.96 | 2.1 | 11.44 | 5.44 | |
| Mg ₀ Co ₁₀₀ -600°C | 50 | -37.56 (4.8mm) | 2.08 | 1.4 | 4.72 | 3.37 | |

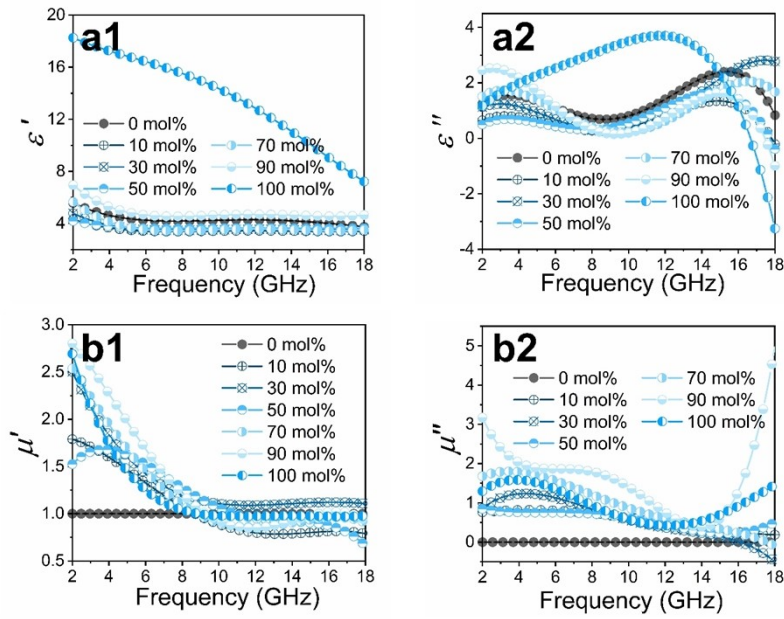


Fig. S6 (a1) The real part (ϵ') and (a2) imaginary part (ϵ'') of relative complex permittivity, (b1) the real part (μ') and (b2) imaginary part (μ'') of relative complex permeability of MgO/Co/C foams formed under various Co^{2+} content (φ , mol%).

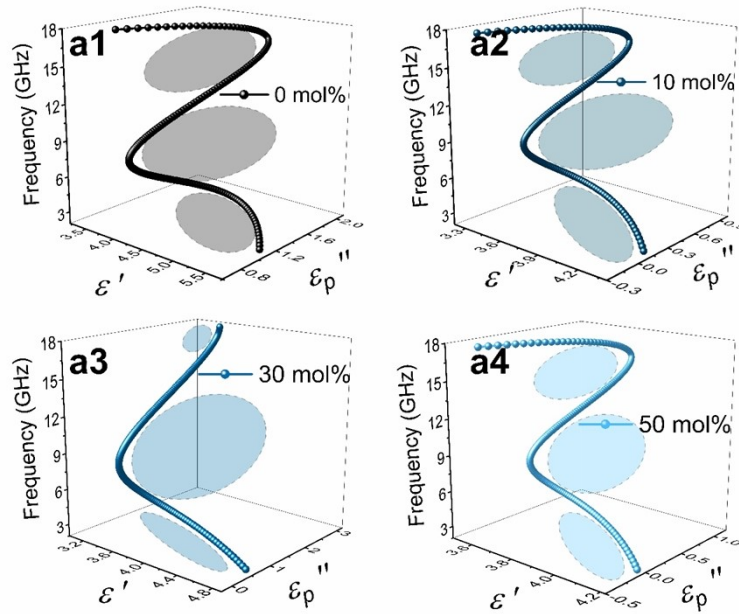


Fig. S7 (a1–a4) Cole–Cole plots (ϵ' versus ϵ_p'') of MgO/Co/C foams formed under various Co^{2+} content (φ , mol%).

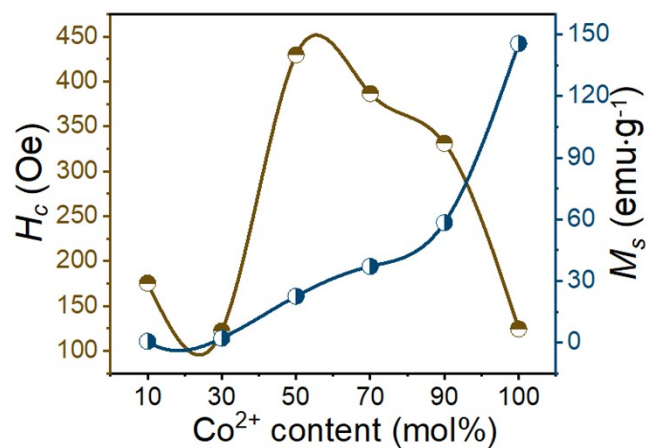


Fig. S8 H_c and M_s of MgO/Co/C foams as a function of Co^{2+} content (φ , mol%).

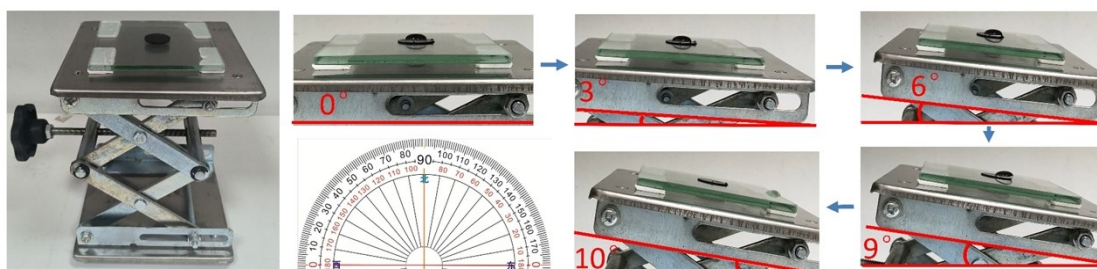


Fig. S9 The droplet rolling test of MgO/Co/C foams ($\varphi = 90$ mol%).

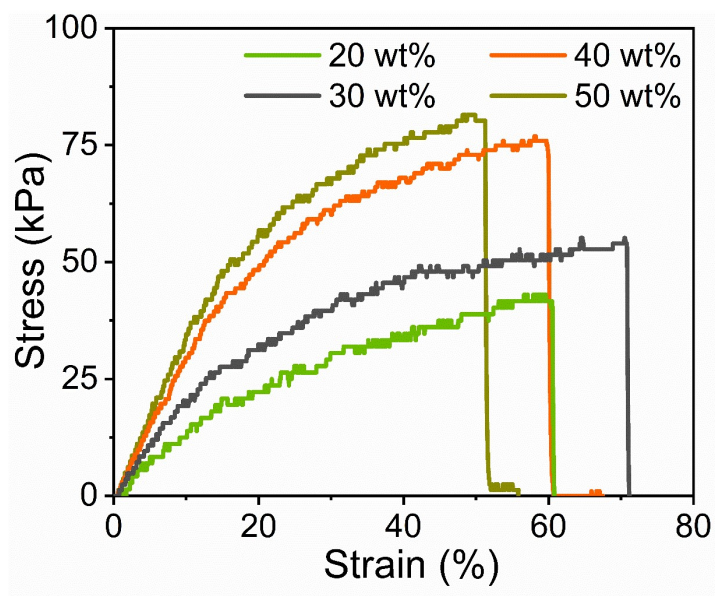


Fig. S10 Stretching stress-strain curves for the MgO/Co/C/silicone films formed under various loading amount ($\varphi = 70$ mol%).